Electromagnetic transitions in ^{13}C and ^{13}N†

R. E. Marrs,* E. G. Adelberger, and K. A. Snover
Department of Physics, University of Washington, Seattle, Washington 98195
(Received 21 March 1977)

The absolute and relative γ-decay strengths of the lowest $T = 3/2$ levels in ^{13}C and ^{13}N are compared using the ^{12}C$(p,\gamma_0)^{13}$N, ^{11}B$(^3$He$,p\gamma)^{13}$C, and ^{11}B$(^3$He$,n\gamma)^{13}$N reactions. By combining the present results with previous measurements, reduced asymmetries of $B(^{13}\mathrm{C})/B(^{13}\mathrm{N}) - 1 = -0.07 \pm 0.13$, $0.82^{+1.2}_{-0.6}$, $\leq 0.83 \pm 0.29$, and -0.04 ± 0.14 are obtained for the $\gamma_0(M1)$, $\gamma_0(E2)$, $\gamma_1(E1)$, and $\gamma_2(M1)$ transitions, respectively. All of the known mirror γ transitions in mass 13 are summarized and compared with theoretical calculations and with the analogous β decays of ^{13}B and ^{13}O. Upper limits of 2–7% are placed on the relative size of the isotensor transition matrix elements for the $M1$ transitions. Changes in the radial wave functions induced by binding energy differences in ^{13}C and ^{13}N do not account for the observed asymmetry of the well known $E1$ decays of the first excited states. This provides clear evidence of charge dependent parentage differences in the T-allowed components of the nuclear wave functions. For the lowest $T = 3/2$ levels in ^{13}C and ^{13}N we find $\Gamma_{\gamma 0}/\Gamma(^{13}\mathrm{C}) = (0.396 \pm 0.030)\%$, $\Gamma_{\gamma 0}/\Gamma_{p0}(^{13}\mathrm{N}) = (12.1 \pm 1.1)\%$, $\Gamma_{p0}\Gamma_{\gamma 0}/\Gamma(^{13}\mathrm{N}) = (5.79 \pm 0.20)$ eV, $\Gamma_{\mathrm{total}}(^{13}\mathrm{C}) = (5.88 \pm 0.81)$ keV, and $\Gamma_{\mathrm{total}}(^{13}\mathrm{N}) = (0.86 \pm 0.12)$ keV. A new efficiency calibration standard at $E_\gamma = 15.1$ MeV is provided by our measurement of the ^{12}C$(p,\gamma_0)^{13}$N thick-target resonant yield, $Y_R = (6.83 \pm 0.22) \times 10^{-9}$ γ_0's per incident proton.

[NUCLEAR REACTIONS ^{12}C(p,γ_0), E = 14.23 MeV resonance; ^{11}B$(^3$He$, p\gamma)$, ^{11}B$(^3$He$, n\gamma)$, particle-γ coincidence; measured Γ_{γ_i}/Γ and deduced Γ_{γ_i} and Γ for ^{13}C ($T = \frac{3}{2}$) and ^{13}N ($T = \frac{3}{2}$); symmetry of mirror transitions.]

I. INTRODUCTION

In recent years mirror nuclei have been used to test the fundamental character of the electromagnetic and weak interactions, and also to determine the accuracy with which corresponding nuclear states are connected by the isospin raising and lower operators. Differences in mirror β-decay ft values, which had been interpreted as possible evidence for second class currents, have largely been explained in terms of charge-dependent differences in the nuclear wave functions.[1] For electromagnetic transitions the experimental situation is less complete. The expected equality of isovector γ transitions in mirror nuclei follows from two assumptions—that the nuclear levels involved obey charge symmetry, and that the electromagnetic current contains only isoscalar and isovector components. To date this equality has been tested only for the $T = \frac{3}{2} \rightarrow T = \frac{1}{2}$ $M1$ transitions in ^{13}C and ^{13}N, from which Blin-Stoyle extracted an upper limit of ~10% for the ratio of isotensor to isovector transition amplitudes.[2] It is possible to check the degree to which the mirror wave functions obey strict charge symmetry by studying mirror $E1$ speeds in $T = \frac{1}{2} \rightarrow T = \frac{1}{2}$ transitions. These are expected to have equal strength in the good isospin limit since the isoscalar $E1$ operator vanishes in the long-wavelength limit, and $\Delta T = 2$ currents cannot connect two $T = \frac{1}{2}$ states. Therefore any violation of mirror symmetry in such transitions must be due to a breakdown of strict charge symmetry in the nuclear wave functions.

We have improved upon previous data concerning the mirror $\Delta T = 1$ decays from the lowest $T = \frac{3}{2}$ levels in mass 13 by significantly increasing the precision of the comparison of the γ_0 and γ_2 $M1$ transitions. We have also extended the comparison to the $E1$ transitions to the first excited states and the $E2$ component of the ground-state transitions. Figure 1 illustrates the transitions which have been measured in the present work.

The summary and comparison of electromagnetic transition strengths in ^{13}C and ^{13}N presented here are derived from a combination of several new measurements, along with existing information. In Sec. II below, our measurement of the ^{12}C(p,γ)-^{13}N yield for the ^{13}N ($T = \frac{3}{2}$) resonance is described. Coincidence measurements of the ^{11}B$(^3$He$, p\gamma)^{13}$C and ^{11}B$(^3$He$, n\gamma)^{13}$N reactions are described in Sec. III. In Sec. IV we compare the observed upper limits on $M1$ asymmetries with those expected from a shell-model calculation of Coulomb and electromagnetic spin-orbit effects,[3] and from a hypothetical isotensor electromagnetic current.[4] The $M1$ transition strengths are also compared with the ft values for the β decays of ^{13}B and ^{13}O, and with the effective-interaction calculations of Cohen and Kurath.[5] Large asymmetries are observed

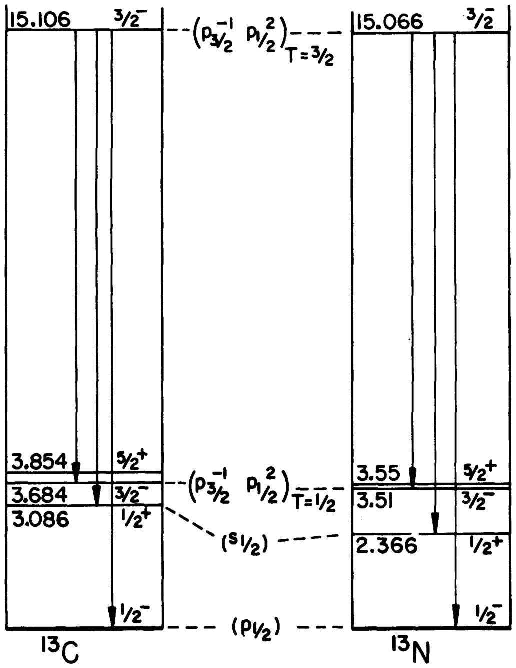

FIG. 1. Level diagrams for ^{13}C and ^{13}N showing the γ-ray transitions measured. The basic shell-model configurations for the different levels are given in parentheses.

in the $E1$ transitions. These are investigated with a model which takes explicit account of changes in radial wave functions caused by binding energy differences between ^{13}C and ^{13}N. Since these effects do not explain the observed asymmetries, we conclude that charge-dependent configuration mixing is required.

An important aspect of the present work is the determination of a new calibration standard for absolute γ-ray detection efficiencies at $E_\gamma = 15$ MeV. A brief account of this work has already been published.[6]

II. $^{12}C(p,\gamma)^{13}N$ YIELD MEASUREMENT

A. Experimental method

We have observed the lowest $T=\frac{3}{2}$ level in ^{13}N as a narrow resonance in the $^{12}C(p,\gamma_0)^{13}N$ reaction.[7] Figure 2 shows γ-ray spectra obtained at proton energies on and off the resonance near $E_p = 14.23$ MeV (lab). The data were obtained by bombarding a self-supporting 1.7-mg/cm^2 natural carbon target with a proton beam from the University of Washington FN tandem Van de Graaff accelerator. γ rays were detected at $\theta_\gamma = 125°$ in a 25-cm × 25-cm NaI spectrometer with a plastic anticoincidence shield.[8] Since the angular distribution of the decay γ rays from an isolated $J=\frac{3}{2}$ level must have the form $A_0P_0(\cos\theta)+A_2P_2(\cos\theta)$ in the center of mass, the total resonance yield can be obtained from the size of the step in a thick-target excitation function obtained at $\theta_\gamma = 125°$, where $P_2(\cos\theta)$ vanishes. In order to enhance the γ-ray counting rate, a large (~15-cm) diameter lead collimator was used with the NaI spectrometer. This resulted in a modest degradation of the energy resolution to ~4.2% full width at half maximum (FWHM) at 15 MeV. The effective solid angle was ~130 msr.

Several different procedures were employed to insure the accuracy of the resonance yield measurements. The effects of dead time and pileup were minimized by running with small beam current; small corrections were made using a pulser whose output was triggered by the beam current integrator and summed with the signal from the

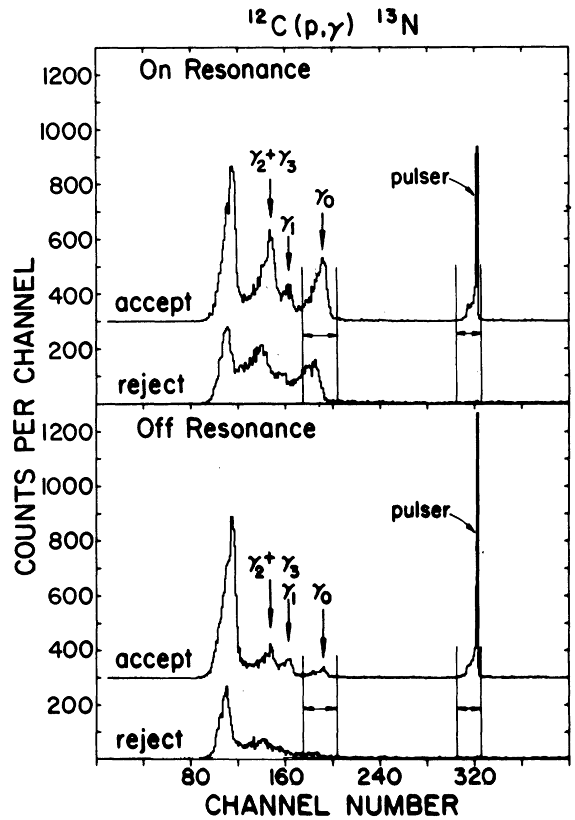

FIG. 2. γ-ray spectra from the $^{12}C(p,\gamma)^{13}N$ measurement obtained at proton energies on and off the ^{13}N ($T=\frac{3}{2}$) resonance at $E_p = 14.23$ MeV. The spectra accepted and rejected by the anticoincidence shield are shown separately, with the accepted spectra displaced by 300 counts. These spectra were obtained with an integrated proton charge of 20 μC accumulated at an average current of 35 nA. The regions summed to obtain the total number of γ_0 and pulser counts are also illustrated. The spectra are cut off at the low-energy end by an electronic discriminator.

phototubes viewing the NaI crystal. The total number of counts in the γ_0 and pulser peaks was determined by summing counts within the windows shown in Fig. 2. The gain was stabilized by an analog device which adjusted the photomultiplier high voltage to keep the 4.44-MeV γ ray at a constant pulse height. The $^{12}C(p,\gamma_0)$ yield per μC of incident protons was determined from the ratio of γ_0 counts to pulser counts. In order to eliminate any possible error from drifts in the discriminator level on the anticoincidence shield, the (p,γ_0) yield was calculated from the sum of the spectra accepted and rejected by the anticoincidence shield after correcting for a small background due to cosmic rays. The current integration system was calibrated with a precision resistor and current source, and the entire 7-m long beam dump including the target chamber was used as a Faraday cup.

The detection efficiency of the NaI spectrometer was calibrated at 15.1 MeV, the energy of the γ_0 transition, using the $^{10}B(^3He,p\gamma)^{12}C$ reaction as explained in Sec. III below. The coincidence yield of 15.1-MeV γ rays from the $^{10}B(^3He,p\gamma)$ reaction was measured at $\theta_\gamma = 125°$ consecutively with the $^{12}C(p,\gamma_0)$ yield measurement. The only alteration in the experimental geometry was to change the target and rotate a proton detector to an angle of 0°.

The resonant γ-ray yield depends on the concentration of ^{12}C in the target. We determined the composition of the target from elastic proton scattering. Figure 3 shows charged particle spectra obtained from the target at laboratory angles of 40° and 120° at a proton energy just below the $E_p = 14.23$-MeV ^{13}N $(T=\frac{3}{2})$ resonance. The particle spectra were accumulated after the completion of the $^{12}C(p,\gamma_0)$ excitation functions. Except for the 1% of ^{13}C in natural carbon, small amounts of hydrogen and oxygen are the only visible contaminants. Using known elastic scattering cross sections for carbon,[9] oxygen,[10] and hydrogen,[11] the effect of these contaminants on the thick-target $^{12}C(p,\gamma)$ yield was determined to be negligible even for the case of a uniform distribution of contaminants through the target interior.

Figure 4 shows the yield of ground-state γ rays per incident proton (multiplied by 4π) obtained at $\theta_\gamma = 125°$ at an average proton current of ~35 nA with 20 μC of integrated beam per point. In order to verify that all of the count-rate-dependent effects were being handled correctly, parts of the excitation function were repeated with a beam current of ~10 nA. As a further check for impurities or irregularities on the target surface, parts of

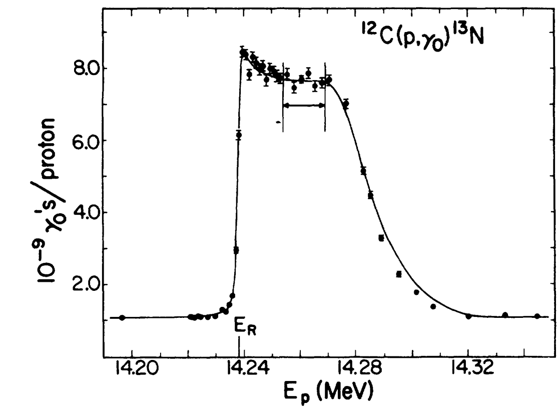

FIG. 4. Resonance yield per incident proton (multiplied by 4π) for the $^{12}C(p,\gamma_0)^{13}N$ reaction at $\theta_\gamma = 125°$. Only statistical errors are shown. There is an additional overall systematic error of ± 3% due to the NaI efficiency calibration. The solid curve is a Monte Carlo calculation (see text). The plateau region used to obtain the thick-target yield is delineated by the vertical lines. Only the $I_p = 35$ nA data are shown here. The energy scale comes from the nominal accelerator calibration.

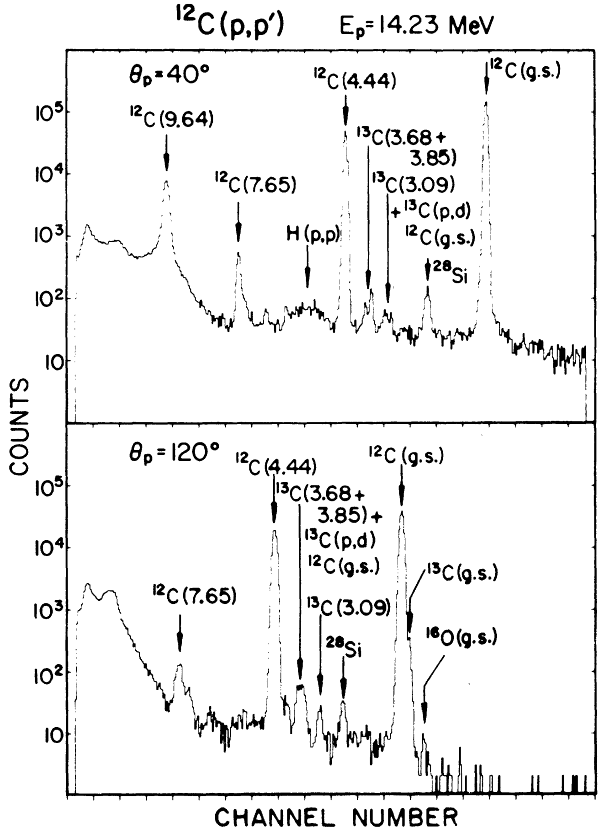

FIG. 3. Charged particle spectra from the 1.7-mg/cm^2 carbon target at a proton energy just below the ^{13}N $(T=\frac{3}{2})$ resonance. The group labeled ^{28}Si corresponds to inelastic scattering in the silicon detector of protons in the ^{12}C (g.s.) group.

the excitation function were repeated again with the target reversed, and at an average current of ~43 nA. The runs at different beam currents gave consistent results, and the weighted average of $Y_{res} = (Y - Y_B) = (6.66 \pm 0.21) \times 10^{-9}$ γ_0's per proton was adopted for the resonant yield (see below) from an infinitely thick natural carbon target. This is 4π times the yield per steradian at $\theta_{lab} = 125°$. The error includes contributions of $\pm\frac{1}{2}\%$ from the statistical uncertainty in the $^{12}C(p, \gamma_0)^{13}N$ data, $\pm 1\%$ from an estimate of the systematic error in the $^{12}C(p, \gamma)$ measurement (including the uncertainty in the beam integration), and $\pm 3\%$ from the accuracy of the $^{10}B(^3He, p\gamma)^{12}C$ calibration. An excitation function was also measured with a thin target in order to check that the nonresonant background was smooth over the energy region spanned by the thick-target yield. No other structure was observed with the thin target between 14.21 and 14.27 MeV.

B. Calculated yield curve

The ~10% overshoot on the leading edge of the thick-target resonance yield curve of Fig. 4, known as the Lewis effect,[12] is due to the discontinuous energy loss of protons in the carbon target. The probability for a proton to lose an amount of energy Q is roughly proportional to $1/Q^2$ up to a maximum value of Q which corresponds to a head-on collision with a free electron. For 14.2-MeV protons the maximum energy loss is $Q_{max} = 4(m_e/m_p)E_p = 31$ keV.

The overshoot can be understood qualitatively[12] by imagining the extreme case in which the stopping power is due entirely to collisions involving an energy loss greater than the resonance width. In this case all protons incident on the target at the resonance energy will have a chance to interact before being degraded in energy, and there will be a maximum in the resonance yield. But if the incident energy is above the resonance energy, some of the protons which suffer hard collisions will jump over the resonance and the overshoot will be damped. Once the beam energy is well above the resonance energy, the thick-target yield approaches a constant value determined by the average stopping power. Calculations of this effect have been made previously for resonances in the neighborhood of $E_p \sim 1$ MeV,[13] and are in agreement with experimental data.

In order to properly interpret our resonance strength measurement, we have investigated the discontinuous-energy-loss effects using the Monte Carlo method of Costello *et al.* and previous authors.[13] The smooth curve in Fig. 4 is a Monte Carlo calculation of the thick-target yield, normalized to the data in the "plateau" region of the yield curve as explained below. The γ-ray yield per proton from a beam of mean energy E_B was calculated from the double convolution integral

$$Y(E_B) = t\int_{E_i=0}^{\infty}\int_{E=0}^{\infty} \sigma(E_R, E)\, g(E_B, E_i) \times \eta(E, E_i)\, dE\, dE_i + Y_B ,$$

where t is the number of target atoms per cm^2 and Y_B is the nonresonant yield. The resonant cross section is

$$\sigma(E_R, E) = \frac{\frac{1}{4}\sigma_0 \Gamma_L{}^2}{(E - E_R)^2 + \frac{1}{4}\Gamma_L{}^2} ,$$

where E_R is the laboratory resonance energy and Γ_L is the laboratory width. $g(E_B, E_i)dE_i$ is the probability that a proton in a beam of mean energy E_B has an energy between E_i and $E_i + dE_i$. A normalized Gaussian distribution was used for $g(E_b, E_i)$. $\eta(E, E_i)$ accounts for the discontinuous-energy-loss effects and is the probability that a proton incident at an energy E_i is found at an energy between E and $E + dE$ somewhere inside the target. The quantity $\eta(E, E_i)$, which for a small range of incident energies depends only on the energy difference $\epsilon = E_i - E$, was calculated from a $1/Q^2$ energy-loss spectrum using Monte Carlo techniques. A computer program was written which followed protons through the target and kept track of the distance traversed within the target (Δx), while the proton energy was within a given interval between ϵ and $\epsilon + \Delta\epsilon$. $\eta(\epsilon)$ was then determined from $\eta(\epsilon) = \Delta x / x\Delta\epsilon$, where x is the total target thickness. The size of the energy bins used was $\Delta\epsilon = 40$ eV.

The energy loss per collision and the path length between collisions were generated from random numbers (R) using the expressions

$$Q = Q_{min}[1 - R(1 - Q_{min}/Q_{max})]^{-1}$$

and

$$\Delta x = -\lambda \ln(1 - R) ,$$

where λ is the mean free path and $0 \le R \le 1$. These expressions distribute the energy losses as $1/Q^2$ and the path lengths as $e^{-\Delta x/\lambda}$. Each proton was followed until its accumulated path length equaled the target thickness.

Previous authors determined the minimum energy loss from the expression $Q_{min} = I^2/Q_{max}$, where I is the average excitation potential for the target material.[13] This makes the average stopping power come out correctly. However, taking I(carbon) ~ 70 eV and Q_{max} as above results in a value of only 0.16 eV for Q_{min}. Since the calculation becomes prohibitive for a Q_{min} this small due to the large number of collisions per proton, a value of

$Q_{\min} = 2$ eV was adopted as an effective minimum-energy transfer to the electrons in carbon. The energy-loss probability was then renormalized to give the correct average stopping power $K_{\rm lab} = 30.75 \pm 0.31$ keV cm^2/mg.[14] This results in a mean energy loss per collision of 19.3 eV and a mean free path of 0.63 μg/cm^2 in carbon. The electron shell effects included in the calculations of Costello *et al.*[13] at lower proton energies were ignored in the present calculation.

A total of 3200 protons were tracked through the target to generate the curve shown in Fig. 4. For this calculation the value of the resonance cross section σ_0 was adjusted to match the observed average plateau yield for the combined yield curves (see above), and the laboratory resonance width was taken to be $\Gamma_{\rm lab} = 930$ eV (see Sec. III below). The target thickness of $x = 1.70$ mg/cm^2 was chosen to reproduce the observed width of the excitation function, and the beam energy resolution of Γ_B (FWHM) = 1.8 keV was chosen to reproduce the slope of the leading edge of the yield curve. Γ_B accounts for both the spread of beam energies and the Doppler broadening of the resonance. The double convolution integral was done numerically. The accuracy of the Monte Carlo calculation in the plateau region was estimated to be ~±0.4% from the fluctuations in the predicted yield.

The excellent agreement between the calculated ^{12}C$(p, \gamma_0)^{13}$N resonant yield and the data gives us confidence that all effects are understood. The quantity most accurately determined by this procedure is $Y_{\rm res} = 6.66 \pm 0.21 \times 10^{-9}$ γ_0's proton, the plateau yield ($\times 4\pi$) that one would measure at θ_γ(lab) = 125° with an infinitely thick natural carbon target. This result is insensitive to the parameters of the calculation, such as the beam energy spread, resonance width, and the stopping power. It is even insensitive to the nature of the energy loss process. If one were to interpret the measured plateau yield (indicated in Fig. 4) in the continuous energy loss approximation (accounting for finite target thickness but neglecting straggling), the extracted value of $Y_{\rm res}$ would be about 0.6% greater than the value given above. This difference depends somewhat on the definition of the plateau region, but in any case is much smaller than the ±3% experimental uncertainty, and could be further reduced by making measurements with a thicker target.

We obtain the resonance strength[15] $Y_R = \pi\sigma_0\Gamma_{\rm lab}/2\epsilon$ after making several small corrections to $Y_{\rm res}$: +1.5% for the lab-to-c.m. solid-angle transformation, and +1.1% to account for the fact that θ_γ (lab) = 125° is not exactly at the zero of $P_2(\cos\theta_{\rm c.m.})$. The measured angular distribution for γ_0 (see Fig. 5 and discussion below) was used in making the second correction. The final result is $Y_R = (6.83 \pm 0.22) \times 10^{-9}$ γ_0's/proton.

It is worth noting the effects of discontinuous energy loss on the apparent resonance energy. The usual considerations (based on continuous energy loss) lead one to expect for a thick target that the resonance energy is the energy at which the resonance yield is one-half of its maximum value. In the present case our calculations indicate the resonance energy lies 0.4 or 0.5 keV lower than the value given by this prescription, depending on whether one takes half the maximum or half the plateau yield.

C. Results

The quantity $\Gamma_{p_0}\Gamma_{\gamma_0}/\Gamma$ was obtained by inserting the usual equation for σ_0 into the formula for Y_R given above:

$$Y_R = \left(\frac{M_1 + M_2}{M_2}\right) \frac{\lambda^2}{2\epsilon} \omega \frac{\Gamma_{p_0}\Gamma_{\gamma_0}}{\Gamma}.$$

Here $Y_R = (6.83 \pm 0.22) \times 10^{-9}$ γ_0's per incident proton as above, $\lambda = 8.22 \times 10^{-13}$ cm is the reduced proton wavelength, and $\epsilon = (2.02 \times 10^{-20}$ mg/

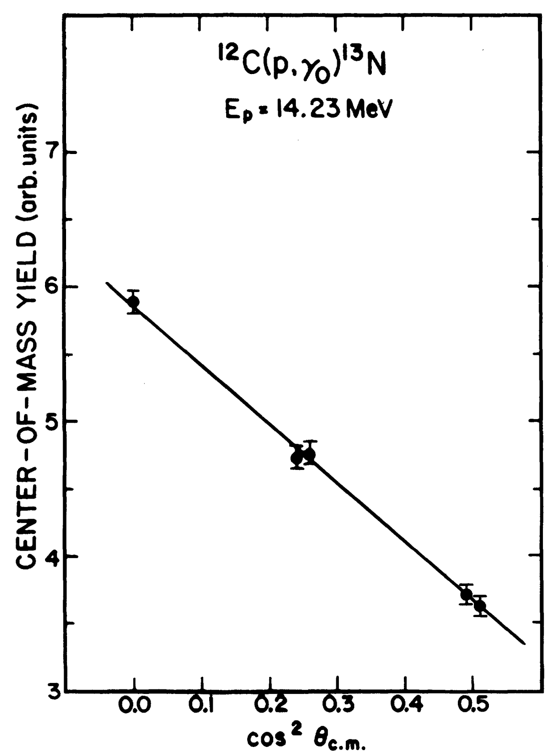

FIG. 5. Angular distribution of the ^{12}C$(p, \gamma_0)^{13}$N resonant yield for the ^{13}N ($T = \frac{3}{2}$) resonance at $E_p = 14.23$ MeV. Yields and angles are with respect to the ^{13}N* reference frame. The nonresonant background has been subtracted. The straight line is a least-squares fit to $A_0P_0(\cos\theta) + A_2P_2(\cos\theta)$.

atom)K_{lab}, where ϵ is the stopping power per ^{12}C atom (of natural carbon) and $K_{lab} = 30.75 \pm 0.31$ keV cm^2/mg.[14] The factor $(M_1 + M_2)/M_2 = \frac{13}{12}$ converts the stopping power to the c.m. system, and the remaining quantities have their usual meaning with all widths given in the c.m. system. The resulting value of $\Gamma_p \Gamma_{\gamma_0}/\Gamma = (5.79 \pm 0.20)$ eV is in agreement with, but more precise than, the previous value of (5.5 ± 0.8) eV.[7] The greater precision obtained here stems primarily from the precise determination of the γ-ray detector efficiency from the proton-γ coincidence measurement, along with a proper accounting for the effects of discontinuous proton-energy loss on the shape of the (p, γ) resonance-yield curve.

Although our value has been obtained by ignoring interference between the resonance and the background, it should not be significantly affected by interference since the ratio of the cross sections $\sigma_0/\sigma_{bkg} \approx 230$, and interferences of $E1$ or $E2$ backgrounds with the $M1$ resonance cannot contribute to the A_0 term in the angular distribution. Our data at $\theta_\gamma = 125°$ measure A_0, since the resonance angular distribution has a negligible A_1 coefficient (see below).

We have determined the $E2/M1$ mixing ratio in the ^{13}N $(T = \frac{3}{2})$ ground-state transition from a measurement of the ^{12}C(p, γ_0) angular distribution at laboratory angles of 45, 60, 90, 120, and 135°. The ^{12}C(p, γ_0) thick-target yield at proton energies above and below the resonance was averaged and subtracted from the resonance yield to obtain the data plotted as a function of $\cos^2\theta_{c.m.}$ in Fig. 5. The straight line in Fig. 5 is a least-squares fit to $A_0 P_0(\cos\theta) + A_2 P_2(\cos\theta)$, from which we determine $A_2/A_0 = -0.68 \pm 0.03$. This implies an $E2/M1$ intensity ratio of 0.013 ± 0.005 in the γ_0 transition. A second fit to the angular distribution with the $P_1(\cos\theta)$ term included yielded a value of $A_1/A_0 = -0.008 \pm 0.014$, confirming that there is no significant contribution to the yield from the P_1 term.

A by-product of the present work is a value for the nonresonant ^{12}C$(p, \gamma_0)^{13}$N cross section at $\theta_\gamma = 125°$ near $E_p = 14.20$ MeV. The result is $\sigma(125°) = 1.1 \pm 0.1$ μb/sr.

III. ^{11}B(^{3}He,$p\gamma$)^{13}C AND ^{11}B(^{3}He,$n\gamma$)^{13}N

A. Experimental method

The relative γ-ray transition strengths from the lowest $T = \frac{3}{2}$ levels in ^{13}C and ^{13}N were compared in a coincidence study of the mirror stripping reactions ^{11}B(^{3}He,$p\gamma$)^{13}C and ^{11}B(^{3}He,$n\gamma$)^{13}N. The experimental arrangement has been described previously.[16] In the present measurements a 150 μg/cm^2, enriched, self-supporting ^{11}B target was

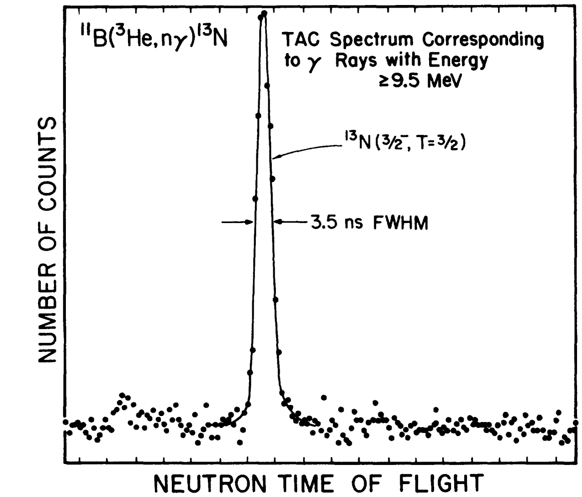

FIG. 6. Neutron time-of-flight spectrum obtained with the ^{11}B(^{3}He,$n\gamma$)^{13}N reaction. Only events with γ-ray signals greater than 9.5 MeV are included.

bombarded with ^{3}He beams of 5.3 MeV for our ^{11}B(^{3}He,$p\gamma$) study and 7.0 MeV for our ^{11}B(^{3}He,$n\gamma$) experiment. γ rays were detected at 125° in the NaI spectrometer, and particles were detected at 0°. The ^{3}He beam was stopped in a stack of nickel and aluminum foils for the proton measurements and in a small tantalum Faraday cup for the neutron measurements. Neutrons were detected in a disc of NE102 plastic scintillator 2.5 cm thick and 11.4 cm in diameter coupled to an RCA4522 photomultiplier tube. The neutron flight path was 35 cm, and the time of flight was measured with respect to coincident γ rays. The data were event-mode recorded and sorted off line.

The neutron time-of-flight spectrum for events with $E_\gamma \geq 9.5$ MeV is shown in Fig. 6. This γ-ray energy range includes all the observed transitions from the lowest $T = \frac{3}{2}$ levels in ^{13}C and ^{13}N. Figure 7 shows a portion of the simultaneously accumulated singles and coincident proton spectra. The area of the proton group populating the ^{13}C $(T = \frac{3}{2})$ state was used to determine a value of $\Gamma_{\gamma_0}/\Gamma = (0.396 \pm 0.030)\%$ for this state. This is smaller than the value of $\Gamma_{\gamma_0}/\Gamma = (0.53 \pm 0.06)\%$ obtained by Cocke *et al.* from a similar measurement.[17] When combined with an electron-scattering measurement[18] of $\Gamma_{\gamma_0} = (23.3 \pm 2.7)$ eV, our measurement yields (5.88 ± 0.81) keV for the total width of the $T = \frac{3}{2}$ level in ^{13}C. This is consistent with, but more precise than, previous values of $\Gamma = (6.0 \pm 1.7)$ keV obtained from a ^{9}Be$(\alpha, \gamma_0)^{13}$C measurement[19] and $\Gamma = 4.7 \pm 1.6$ keV derived by Cocke *et al.*[17]

We also measured $\Gamma_{\gamma_0}/\Gamma_{p_0}$ for ^{13}N $(T = \frac{3}{2})$. In a separate measurement we detected neutron-proton

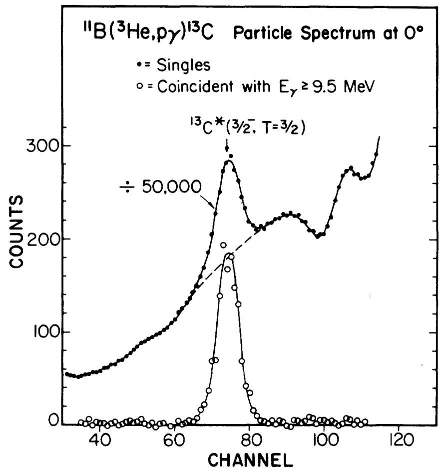

FIG. 7. The ^{11}B(^{3}He,$p\gamma$)^{13}C singles proton spectrum at $\theta_p = 0°$ and the coincidence spectrum corresponding to events with γ-ray signals greater than 9.5 MeV. The solid lines are drawn to indicate the singles and coincidence line shapes, which are the same if the background shown by the broken line is assumed for the singles data.

coincidences associated with this level. Then $\Gamma_{\gamma_0}/\Gamma_{p_0}$ is given by the ratio of the neutron-γ coincidence yield (as described above) to the neutron-proton coincidence yield, where in each case these yields were normalized to the yield of the ^{13}C$_{g.s.}$ proton group observed in a monitor detector. The particle spectrum obtained in the monitor detector at 40°(lab) is shown in Fig. 8. The monitor detector was covered by a 9.4 mg/cm^2 aluminum foil to stop elastic ^{3}He particles.

Coincident protons from the decay of ^{13}N ($T = \frac{3}{2}$)

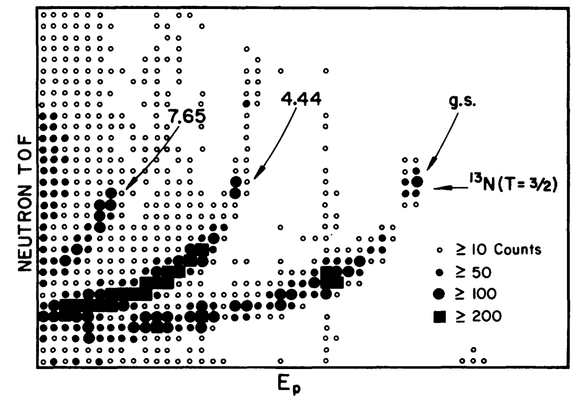

FIG. 9. Example of data obtained in the ^{11}B(^{3}He,np)^{12}C measurement. The diagonal arrows indicate kinematic bands corresponding to levels in ^{12}C. The ^{13}N ($T = \frac{3}{2}$) enhancement occurs at a fixed neutron time of flight.

were detected in a telescope consisting of a 200-μm surface-barrier detector and a 2.4-mm thick silicon detector at a laboratory angle of 117°. A solid angle of 45 msr was defined by a circular aperture covered with 4.7 mg/cm^2 of aluminum foil to stop ^{3}He and α particles. An example of the neutron-proton coincidence data is shown in Fig. 9. The determination of the ground-state proton yield is straightforward. The position of the low-level cutoff in the neutron energy spectrum was carefully monitored by counting an ^{241}Am source at the beginning and end of each data run. The position of the 60-keV photopeak was used to establish a digital threshold on the slow energy signal from the scintillator as illustrated in Fig. 10. From this procedure we obtain $\Gamma_{\gamma_0}/\Gamma_{p_0} = (12.1$

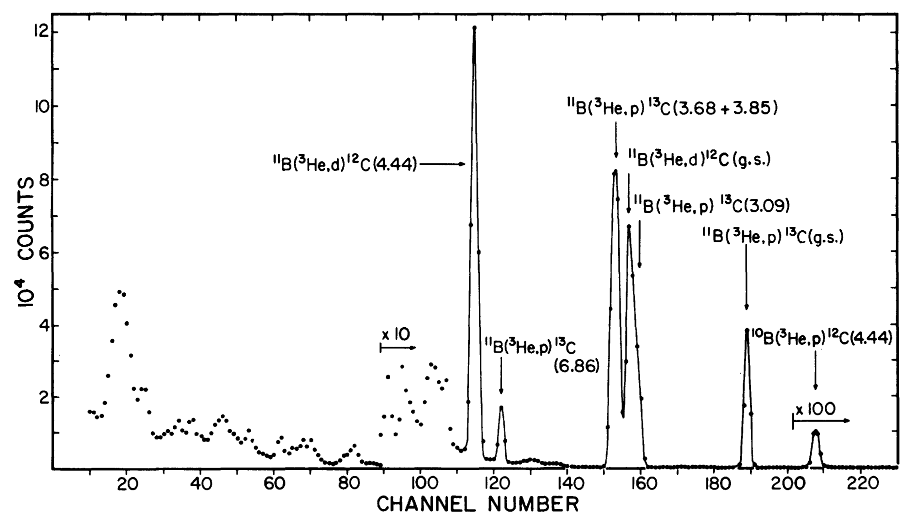

FIG. 8. Spectrum obtained in the monitor detector at an angle of 40° (lab) and a ^{3}He energy of 7.0 MeV. The group labeled ^{11}B(^{3}He,p)^{13}C (g.s.) was used to monitor the number of ^{11}B + ^{3}He interactions in the target.

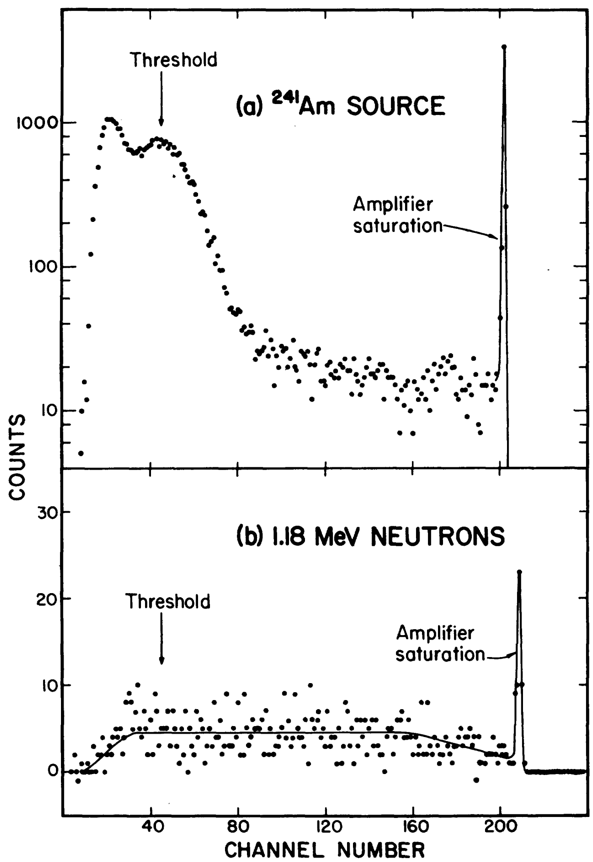

FIG. 10. (a) Response of the neutron detector to an ^{241}Am source. The arrow corresponds to the location of the 60-keV photopeak, which was used to set a digital threshold during the data analysis (see text). (b) Response of the detector to 1.18-MeV neutrons which populate the lowest $T=\frac{3}{2}$ level in ^{13}N. The solid curve is drawn only to guide the eye. Random events have been subtracted.

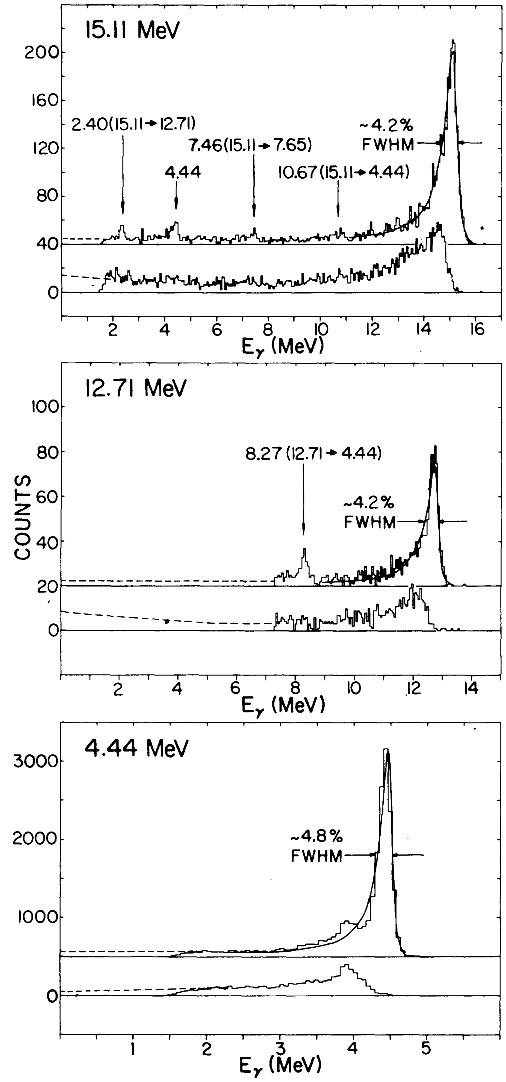

FIG. 11. Response of the NaI spectrometer to γ rays of different energies. Spectra accepted by the anticoincidence shield are displaced upward. The 15.11- and 4.44-MeV spectra are cut off at ~1.5 MeV by a discriminator threshold. The 12.71-MeV spectrum is not shown below ~7 MeV due to the presence of strong background γ rays.

± 1.1)%, which is consistent with a previous measurement of (12 ± 2)%.[17]

B. NaI calibration

The 1^+, $T=1$ level at 15.11 MeV in ^{12}C decays predominantly by a γ transition to the ground state and therefore offers a unique opportunity to calibrate the NaI spectrometer at virtually the same energy as the γ_0 transitions from the lowest $T=\frac{3}{2}$ levels in ^{13}C and ^{13}N. The efficiency-solid-angle product of the NaI spectrometer was determined at $E_\gamma = 15$ MeV by observing tagged γ rays from the ^{10}B(^{3}He,$p\gamma$)^{12}C reaction (see Ref. 16). An enriched, 150-μg/cm^2 ^{10}B target was bombarded with a 4.1-MeV ^{3}He beam and coincident protons were detected at 0° using the same setup employed for the ^{11}B(^{3}He,p)^{13}C measurement. Since the p-γ angular correlation for a $J=1$ level must also be of the form $A_0P_0(\cos\theta)+A_2P_2(\cos\theta)$, γ rays were detected at 125°, where $P_2(\cos\theta)$ has a zero.

Figure 11 shows the coincident 15.11-MeV γ-ray line shape, as well as line shapes at $E_\gamma = 12.71$ and 4.44 MeV. The 4.44-MeV line shape was obtained by setting a window on the proton group populating the first excited state of ^{12}C, and the 12.71-MeV line shape was obtained from ^{11}B(^{3}He,$d\gamma$)^{12}C data accumulated simultaneously with the ^{11}B(^{3}He,$p\gamma$)^{13}C data.

A smooth line shape having a constant precentage width was derived from the 15.11-MeV data of Fig.

11, and was fitted to all of the γ-ray spectra reported in the present work in order to obtain γ-ray yields and energies. The smooth curves in Fig. 11 are examples of the fitting procedure. It can be seen that the percentage energy resolution of the NaI spectrometer is essentially constant for the γ-ray energies of interest in the ^{13}C-^{13}N comparison. The low energy tails of the line shape (below ~$0.7E_\gamma$) were not included in the fitting procedure.

In determining the γ detection efficiency a branching ratio of $\Gamma_{\gamma_0}/\Gamma = (88.2 \pm 2.1)\%$ was adopted for ^{12}C(15.11) based on existing measurements of the α-decay[20] and relative γ-decay[21] branching ratios. The NaI efficiency was extrapolated to lower energies using γ-ray absorption coefficients and the observed energy dependence of the accepted and rejected line shapes. The uncertainty in the NaI efficiency makes a negligible contribution to the error in the relative γ-ray transition strengths reported for ^{13}C and ^{13}N, since the transitions have nearly the same energy in both nuclei.

C. Results

The coincident γ-ray spectra corresponding to the deexcitation of the lowest $T=\frac{3}{2}$ levels in ^{13}C and ^{13}N are shown in Fig. 12 together with the least-squares-fitted line shapes. A small background due to random coincidences has been subtracted. The γ-ray widths, branching ratios, and total widths obtained for the $\frac{3}{2}^-$, $T=\frac{3}{2}$ levels in ^{13}C and ^{13}N are summarized in Table I. Γ_{γ_0} for ^{13}C is taken from the electron scattering measurement of Wittwer, Clerc, and Beer,[18] while Γ_{γ_0} for ^{13}N is obtained from the present measurement of

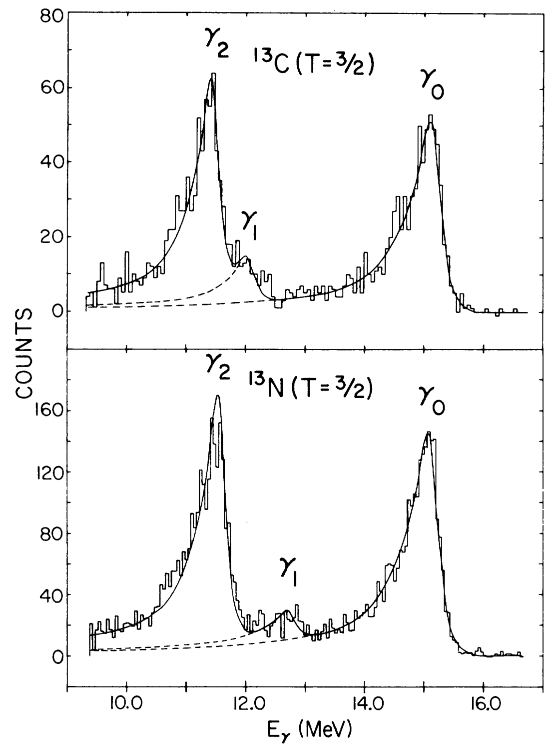

FIG. 12. Coincident γ-ray spectra from the decay of the $T=\frac{3}{2}$ levels in ^{13}C and ^{13}N. The smooth curves are least-squares-fitted line shapes.

$\Gamma_{p_0}\Gamma_{\gamma_0}/\Gamma$ in combination with a previous coincidence measurement[22] of $\Gamma_{p_0}/\Gamma = 0.236 \pm 0.012$.

The unresolved transition to the $\frac{3}{2}^-$ and $\frac{5}{2}^+$ second and third excited states is expected to go predominantly to the $\frac{3}{2}^-$ level. In ^{13}N these transitions

TABLE I. Summary of γ widths (in eV) and branching ratios for the ^{13}C($\frac{3}{2}^-$, $T=\frac{3}{2}$) and ^{13}N-($\frac{3}{2}^-$, $T=\frac{3}{2}$) levels at $E_x = 15.1$ MeV. The state labeled $\frac{5}{2}^-$ refers to the level at 7.55 MeV in ^{13}C.

J^π of final state	^{13}C	Γ_γ (eV) ^{13}N	Theory (^{13}N)[a]
$\frac{1}{2}^-$(g.s.)	$22.7 \pm 2.6(M1)$[b]	$24.2 \pm 1.5(M1)$	$26.24(M1)$
	$0.59 \pm 0.11(E2)$[b]	$0.32 \pm 0.12(E2)$	$0.74(E2)$
$\frac{1}{2}^+$	4.12 ± 0.74	$\leq 2.82 \pm 0.30$	
$\frac{3}{2}^- + \frac{5}{2}^+$	18.2 ± 2.4	19.6 ± 1.4	10.44 (to $\frac{3}{2}^-$)
$\frac{5}{2}^-$	<0.9		7.0×10^{-3}

Decay properties of the $T=\frac{3}{2}$ levels

^{13}C	^{13}N
$\Gamma_{\gamma_0}/\Gamma = (0.396 \pm 0.030)\%$	$\Gamma_{p_0}\Gamma_{\gamma_0}/\Gamma = (5.79 \pm 0.20)$ eV
$\Gamma = (5.88 \pm 0.81)$ keV	$\Gamma_{\gamma_0}/\Gamma_{p_0} = (12.1 \pm 1.1)\%$
	$\Gamma = (0.86 \pm 0.12)$ keV

[a] Reference 32.
[b] Reference 18.

are not resolved, while in ^{13}C the 170-keV energy separation allows us to place an upper limit of 20% on the $\frac{5}{2}^+$ contribution by use of the line-shape fitting procedure. The presence of a weak $E1$ transition to the $\frac{5}{2}^+$ state would not substantially alter our conclusion, since $E1$ and $M1$ transitions have the same energy dependence and are both expected to have equal strength in ^{13}C and ^{13}N.

Although the natural line widths of the unbound states in ^{13}N are much smaller than our instrumental resolution, the systematic errors in Γ_{γ_1} and Γ_{γ_2} introduced by the tails of the unbound levels were estimated from their resonance shape seen[23] in ^{12}C(p,γ) adjusted by the appropriate $E_\gamma{}^3$ phase-space factors. The γ_1 and γ_2 strength "missed" by the line-shape fitting program was found to be much smaller than our statistical uncertainties and has been neglected.

The 12.71-MeV γ_1 transition in ^{13}N may contain an unresolved contribution from the γ decay of ^{12}C (12.71) populated in the proton decay of the ^{13}N $(T=\frac{3}{2})$ level. We estimate the contribution of 12.71-MeV γ rays from this process as follows. ^{12}C $(12.71, T=0)$ contains[16] a $\beta^2=(0.21\pm0.11)\%$ admixture of ^{12}C $(15.1, T=1)$. The $T=\frac{3}{2}$ level in ^{13}N should decay strongly to the ^{12}C (15.1) impurity in the 12.71-MeV state. We estimate the partial width for this decay as $\Gamma_p = 2P\gamma_{\rm WL}{}^2C^2S\beta^2$, where P is a Coulomb penetration factor, $\gamma_{\rm WL}{}^2$ is the Wigner-limit width, C is an isospin Clebsch-Gordan coefficient, and S is the spectroscopic factor for ^{13}B (g.s.) $\rightarrow$ ^{12}B (g.s.) $+n$. Using the Cohen-Kurath value[24] of $S=0.629$ and Γ_{γ_0}/Γ (^{12}C) (12.71) $=(1.93\pm0.12)\%$ from Ref. 16, we expect that the isospin forbidden proton decays are responsible for $(15\pm8)\%$ of the "γ_1" yield. Hence Γ_{γ_1} for ^{13}N $(T=\frac{3}{2})$ is given in Table I as an upper limit.

The total width of ^{13}N (15.07) can be obtained from $\Gamma=(\Gamma_{\gamma_0}/\Gamma_{p_0})^{-1}\times(\Gamma_{p_0}\Gamma_{\gamma_0}/\Gamma)(\Gamma_{p_0}/\Gamma)^{-2}$. From our measurements of the first two ratios and the value of Γ_{p_0}/Γ given in Ref. 22, we obtain $\Gamma=(860\pm120)$ eV.

Recently Hinterberger *et al.*[25] made a careful study of the ^{12}C(p,p) reaction over the 14-MeV $T=\frac{3}{2}$ resonance. They obtain $\Gamma_{p_0}/\Gamma=0.191\pm0.017$ and $\Gamma=1.10\pm0.09$ keV, which when combined with our value for $\Gamma_{p_0}\Gamma_{\gamma_0}/\Gamma$ yield $\Gamma_{\gamma_0}=30.3\pm2.9$ eV. Since these results disagree with our values we have tried to account for the discrepancy. It is interesting to note that the value of $\Gamma_{p_0}=203\pm22$ eV derived from our work and Ref. 22 agrees well with $\Gamma_{p_0}=210\pm11$ eV obtained by Hinterberger *et al.*[25] An elastic scattering interference anomaly is sensitive primarily to Γ_{p_0} when $\Gamma\lesssim R$, where R is the experimental energy resolution. If Hinterberger *et al.* had slightly underestimated R the effect would be to yield an erroneously large value of Γ and hence an erroneously small value of Γ_{p_0}/Γ. Although we cannot find any fault with the analysis of Ref. 25, the history of elastic scattering studies of very narrow resonances indicates that it is difficult to compute resolution functions correctly.

IV. COMPARISON OF TRANSITION STRENGTHS

A. $M1$ transitions

The six known mirror electromagnetic transitions in ^{13}C and ^{13}N are listed in Table II. The reduced transition strengths are expressed in Weisskopf units (W.u.); and the measurements are from the present work unless noted otherwise. For the purpose of comparing the reduced transition strengths in ^{13}C and ^{13}N it is convenient to define the asymmetry parameter $\delta\equiv B(^{13}\mathrm{C})/B(^{13}\mathrm{N})-1$, which also appears in Table II. The precision of our comparison of the $\Delta T=1$, $M1$ transitions is improved by defining the relative asymmetry $\Delta\equiv B_{\gamma_2}(^{13}\mathrm{C})B_{\gamma_0}(^{13}\mathrm{N})/B_{\gamma_0}(^{13}\mathrm{C})B_{\gamma_2}(^{13}\mathrm{N})-1$. Δ can be determined accurately since it is independent of the absolute strengths.

Since the $M1$ operator contains no radial dependence in the long-wavelength limit, and the γ_0 and γ_2 transitions are strong, these transitions are relatively insensitive to differences in the nuclear structure and hence test the structure of the electromagnetic current itself. Defining A_2 and A_1 as the reduced isotensor and isovector transition amplitudes, respectively, a nonzero isotensor amplitude would produce an asymmetry of $\delta=4(\frac{3}{5})^{1/2}A_2/A_1$ for each of the "isovector" transitions, and a relative asymmetry of $\Delta=8(\frac{3}{5})^{1/2}\bar{A}$ for the two $M1$ transitions. Here $\bar{A}\equiv\frac{1}{2}[A_2/A_1(\gamma_2)-A_2/A_1(\gamma_0)]$. The $M1$ transitions are seen to have no asymmetry within the experimental uncertainties, and upper limits (at 68% confidence level) are given for A_2/A_1 and $\bar{A}$ in Table II.

The $\Delta T=1$ transition strengths may also be affected by charge-dependent mixing in the initial or final states. Table II lists the asymmetry δ in the γ_0 transition predicted by the shell-model calculation of Sato and Yoshida,[3] which included Coulomb and electromagnetic spin-orbit effects. The predicted asymmetry from these effects is smaller than our experimental upper limit.

The asymmetries in the $M1$ transitions expected from a hypothetical isotensor electromagnetic current, as calculated by Chemtob and Furui,[4] are also displayed in Table II. These asymmetries are also smaller than our experimental upper limits. Even though our experimental results have placed a good limit on the reduced isotensor matrix element A_2, the corresponding limit for the isotensor

TABLE II. Comparison of reduced transition strengths in ^{13}C and ^{13}N. $\delta \equiv B(^{13}\mathrm{C})/B(^{13}\mathrm{N}) - 1$.

	E_i	(J^π, T)	E_f	(J^π, T)	B (W.u.)		δ (exp.)	δ (theory)	$\lvert A_2/A_1 \rvert$
^{13}C	15.11	$(\frac{3}{2}^-, \frac{3}{2})$	0.0	$(\frac{1}{2}^-, \frac{1}{2})$	0.318 ± 0.036 [a]	$(M1)$	-0.07 ± 0.13	0.01 [b]	<0.065
^{13}N	15.07		0.0		0.342 ± 0.021			-0.049 [c]	
^{13}C	15.11	$(\frac{3}{2}^-, \frac{3}{2})$	0.0	$(\frac{1}{2}^-, \frac{1}{2})$	0.51 ± 0.10 [a]	$(E2)$	$0.82^{+1.2}_{-0.6}$		
^{13}N	15.07		0.0		0.28 ± 0.11				
^{13}C	15.11	$(\frac{3}{2}^-, \frac{3}{2})$	3.68	$(\frac{3}{2}^-, \frac{1}{2})$	0.587 ± 0.077 [d]	$(M1)$	-0.04 ± 0.14	0.003 [b]	<0.058
^{13}N	15.07		3.51		0.613 ± 0.044 [d]				
^{13}C	15.11	$(\frac{3}{2}^-, \frac{3}{2})$	3.09	$(\frac{1}{2}^+, \frac{1}{2})$	$(6.4 \pm 1.1) \times 10^{-3}$	$(E1)$	$\geq 0.83 \pm 0.29$		
^{13}N	15.07		2.37		$\leq (3.69 \pm 0.39) \times 10^{-3}$				
^{13}C	3.68	$(\frac{3}{2}^-, \frac{1}{2})$	3.09	$(\frac{1}{2}^+, \frac{1}{2})$	0.038 ± 0.011 [e]	$(E1)$	-0.60 ± 0.13		
^{13}N	3.51		2.37		0.094 ± 0.013 [f]				
^{13}C	3.09	$(\frac{1}{2}^+, \frac{1}{2})$	0.0	$(\frac{1}{2}^-, \frac{1}{2})$	0.040 ± 0.005 [g]	$(E1)$	-0.69 ± 0.05		
^{13}N	2.37		0.0		0.13 ± 0.01 [h]				
							$\Delta = 0.03 \pm 0.07$ [i]	-0.007 [b]	$\bar{A} < 0.016$ [i]

[a] Reference 18.
[b] Isotensor, Ref. 4.
[c] Charge dependent, shell model, Ref. 3.
[d] This may contain a small unresolved component (see text).
[e] Reference 33 as quoted in Ref. 23.
[f] Reference 23.
[g] Reference 34.
[h] Weighted average as given in Ref. 35.
[i] See text.

current is not very stringent, since its effects in nuclei are highly suppressed because a $\Delta T = 2$ current cannot couple to single nucleons. Upper limits on the isotensor amplitude have also been obtained in searches for isospin forbidden ($\Delta T = 2$) γ transitions[26] and in various high energy experiments.[27]

The β decays of ^{13}B (Refs. 28 and 29) and ^{13}O (Ref. 30) are analogous to the isovector $M1$ decays of the lowest $T = \frac{3}{2}$ levels in ^{13}C and ^{13}N if the orbital part of the $M1$ operator is neglected. An asymmetry in the mass-13 β decays of $\delta_\beta = ft^+/ft^- - 1 = 0.166 \pm 0.026$ has been observed experimentally.[28,30] As in the mirror γ decays, the asymmetry δ_β could be due either to charge-dependent differences in the nuclear wave functions or to a fundamental effect such as a second class current. Although the charge-dependent shell-model calculations of Sato and Yoshida[3] predict a β-decay asymmetry δ_β of only 0.047, one cannot conclude that charge-dependent effects are not responsible for the entire asymmetry. Unfortunately, the experimental uncertainty of ± 0.13 in the γ_0 asymmetry makes a quantitative comparison of the observed β and γ asymmetries impossible.

The importance of the orbital contribution to the $\Delta T = 1$ $M1$ matrix elements may be assessed by comparing the absolute value of the analogous β and γ transition strengths. Since the small asymmetries δ_β and δ_γ are not of interest here, we average the experimental logft values for ^{13}B and ^{13}O, and the reduced transition strengths for ^{13}C and ^{13}N. These averaged strengths are compared in Table III. Here the γ-ray transition strengths $\Lambda_\gamma(M1)$ are obtained from the expression $\Lambda_\gamma(M1) = 362\Gamma_\gamma(\mathrm{eV})/E_\gamma^3(\mathrm{MeV})$. We follow Ref. 31 and define the γ-ray transition strength expected on the basis of the β-decay strength as $\Lambda_\beta(M1) = 11.1C\Lambda(\mathrm{GT})$, where $\Lambda(\mathrm{GT}) = 4390/ft$, and C is the square of the ratio of the isospin Clebsch-Gordan coefficients for the γ and β transitions. In the present case $C = \frac{2}{3}$. The spin component of the $M1$ transition, which is measured by the analogous β decays, is in reasonable agreement with the experimental strengths for the ground-state transition, but accounts for only 25% of the transition strength to the $\frac{3}{2}^-$ state. The importance of the orbital term in the analog-to-antianalog transition and the sensitivity of this strength to the details of the antianalog wave function have been pointed out previously by Dietrich *et al.*,[7] who computed the transition strength in a simple j-j coupling model with the orbital term included. The $M1$ and $E2$ transition strengths predicted[32] in the Cohen-Kurath $1p$ shell calculation are listed in Table I. The failure of the Cohen-Kurath calculation to reproduce the analog-to-antianalog transition strength presumably results from this extreme sensitivity.

B. $E1$ and $E2$ transitions

Unlike the $M1$ transitions, the $E1$ decays of the $T = \frac{3}{2}$ level display a pronounced charge asymmetry. Similar asymmetries are observed in all the known

TABLE III. Comparison of the average isovector $M1$ transition strengths in ^{13}C and ^{13}N with the average β-decay strengths of ^{13}B and ^{13}O to the same final states. $\Lambda_\beta(M1)$ is the expected $M1$ strength obtained from the β-decay ft values.

Final $T=\frac{1}{2}$ state J^π	$E_x(^{13}C)$	Logft ^{13}B [a]	^{13}O [b]	$\Lambda_\beta(M1)$ [c]	$\Lambda_\gamma(M1)_{exp}$ [d]	$\Lambda_\gamma(M1)_{theory}$ [e]
$\frac{1}{2}^-$	0.00	4.04 ± 0.01	4.10 ± 0.02	2.90 ± 0.06	2.51 ± 0.14	2.78
$\frac{3}{2}^-$	3.68	4.45 ± 0.05	4.52 ± 0.13	1.13 ± 0.12	4.56 ± 0.29	2.45
$\frac{5}{2}^-$	7.55	5.33 ± 0.09	5.22 ± 0.23	0.16 ± 0.04	<0.8	5.6×10^{-3}

[a] References 28 and 29 as given in Ref. 30.
[b] Reference 30.
[c] Based on weighted average of logft for ^{13}B and ^{13}O.
[d] Present work, weighted average of ^{13}C and ^{13}N.
[e] Reference 32.

mirror $E1$ decays from $T=\frac{1}{2}$ levels in mass 13[23,33-35] (see Table II). There is also a suggestion of an asymmetry in the $E2$ component of the γ_0 transition from the $T=\frac{3}{2}$ level. In two of the three $E1$ transitions a $\Delta T=2$ current cannot produce an asymmetry because it does not connect $T=\frac{1}{2}$ levels. The asymmetry in the weak $E1$ transition from the $T=\frac{3}{2}$ level probably should not be attributed to an isotensor current either. We must look to the nuclear structure for an explanation of the asymmetries in the electric transitions.

First we consider isospin mixing as a source of the asymmetries. For the $\frac{1}{2}^+$, $T=\frac{1}{2}$ ground-state decays the isospin impurity amplitude $\beta \leq 0.1$ MeV/15 MeV $\sim 7\times10^{-3}$, where 0.1 MeV is a large isospin mixing element and 15 MeV is roughly the minimum size for a $T=\frac{3}{2}$ to $T=\frac{1}{2}$ energy denominator. If the admixed state has a strong (~0.1 W. u.) $E1$ decay, then this would cause a $\sim 2\beta = 1\%$ effect on the observed transitions. For the $T=\frac{3}{2}$ levels, none of the isospin-forbidden particle decay widths exceeds 10^{-4} single-particle units, and most have $\sim 10^{-5}$ single-particle units.[22] A $T=\frac{1}{2}$ admixture with strong intrinsic γ (0.1 W.u.) and particle ($\theta^2=0.1$) decays would change the $E1$ strength by ~25% if it were admixed with the maximum amplitude permitted by the observed particle decays. Therefore isospin mixing cannot be responsible for the asymmetries of the $T=\frac{1}{2}$ levels and is apparently not the sole cause of the $T=\frac{3}{2}$ asymmetries either.

We next inquire whether binding-energy effects can be responsible for the asymmetries. Each of the $E1$ transitions involves the $\frac{1}{2}^+$ first excited state, which is bound by 1861 keV in ^{13}C and unbound by 422 keV in ^{13}N. Since the radial wave function of the 2.37-MeV state of ^{13}N will "stick out" farther than the wave function of the analog 3.09-MeV state of ^{13}C, one might expect some differences in mirror transitions involving these levels. We have calculated the transition strength for both the $(\frac{1}{2}^+, T=\frac{1}{2}) \to (\frac{1}{2}^-, T=\frac{1}{2})$ and the $(\frac{3}{2}^-, T=\frac{3}{2}) \to (\frac{1}{2}^+, T=\frac{1}{2})$ $E1$ transitions in a simple one-particle model with a single configuration for each state. We are led to this approximation since the $\frac{1}{2}^+$ states are almost pure $2s_{1/2}$ single-particle states (see below). Single-particle radial wave functions were generated in a nucleon-plus-^{12}C central potential of the form

$$V(r)=V_{Re}f(r)-V_{so}\left(\frac{\hbar}{m_\pi c}\right)^2\frac{1}{r}\left|\frac{d}{dr}f(r)\right|\sigma\cdot\vec{l}+V_C(r),$$

where $f(r)=[1+e^{(r-R_0)/a}]^{-1}$, and $V_C(r)$ is the Coulomb potential of a uniformly charged sphere of radius $R_0=r_0A^{1/3}$. The radial wave functions were calculated with the computer code ABACUS.[36] The real well depth, V_{Re} was adjusted separately for ^{13}C and ^{13}N to obtain the correct binding energies, and the other parameters were held fixed. No imaginary terms were included in the potential. The well depths used are listed in Table IV, and the resulting wave functions are plotted in Fig. 13. The largest neutron-proton asymmetry occurs in the $^{12}C(0^+)\otimes 2s_{1/2}$ wave function, which is unbound in ^{13}N. Our purpose is to compute the direct effect of this binding difference upon the $E1$ transition rates.

The strength of the $\frac{1}{2}^+ \to \frac{1}{2}^-$ transition in ^{13}C was computed from the expression[37] $\Gamma_\gamma(E1)=\frac{4}{9}e^2\alpha^2(E_\gamma/\hbar c)^3 SR\theta_i^2\theta_f^2$. The strength of the mirror transition in ^{13}N was calculated in two steps. First the resonant cross section was computed from the expression[38] $\sigma(E1)=(8\pi/3)(E_\gamma/\hbar c)^3(e^2/\hbar v)\alpha^2 S'R'\theta_i^2\theta_f^2$, and then $\sigma(E1)$ was integrated over the resonance. In these expressions the effective charge $\alpha=\pm\frac{1}{2}(\frac{12}{13})$. The statistical factors, which account for the angular momentum algebra, are $S=1$ and $S'=\frac{2}{3}$. The spectroscopic factors for the initial and final

TABLE IV. Real-well depths used to generate the wave functions for the calculations of the single-particle $E1$ transition strengths in ^{13}C and ^{13}N. Other parameters (held constant) in the potential were $r_0 = 1.25$ fm, $a = 0.65$ fm, $V_{so} = 5.5$ MeV. Positive binding energy (E_B) indicates an unbound configuration. The labels "neutron" and "proton" indicate that the binding energy is with respect to the level in ^{13}C or ^{13}N, respectively.

J^π	Parentage	E_B (MeV) Neutron	E_B (MeV) Proton	V_{Re} (MeV) Neutron	V_{Re} (MeV) Proton
$\frac{1}{2}^-$	$^{12}C(0^+)\otimes 1p_{1/2}$	−4.947	−1.944	43.916	44.004
$\frac{1}{2}^+$	$^{12}C(0^+)\otimes 2s_{1/2}$	−1.861	+0.422	57.534	56.875
$\frac{3}{2}^-(T=\frac{3}{2})$	$^{12}C(2^-, T=1)\otimes 2s_{1/2}$	−6.418	−3.455	70.761	70.276

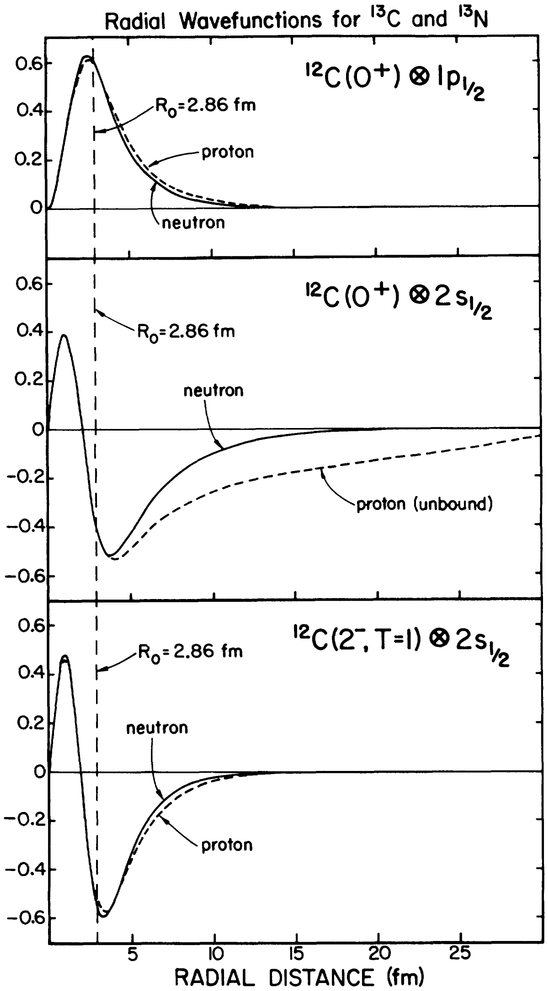

FIG. 13. Radial wave functions for single-particle configurations in mass 13 computed using a Woods-Saxon potential. The quantity plotted is $u(r) = r\psi(r)$. For the unbound proton corresponding to the first excited state of ^{13}N, $u(r)$ has been normalized to the ^{13}C wave function inside the nuclear radius for display purposes only. Aside from the normalization, $u(r)$ is equal to the $2s_{1/2}$ component of the ^{12}C + p scattering wave function computed on the peak of the ^{13}N($\frac{1}{2}^+$) resonance.

states, $\theta_i^2 = 1.02$ and $\theta_f^2 = 0.49$,[23] were assumed to be the same in ^{13}C and ^{13}N. R and R' are the squares of the radial integrals from $r = 0$ to 30 fm as calculated by ABACUS, and v is the relative proton velocity. The resonance shape for $\sigma(E1)$ was calculated by stepping the proton energy over the resonance while holding the potential fixed. The result is compared with a Breit-Wigner shape in Fig. 14. The good agreement[23] means that the Breit-Wigner formula with $\Gamma = 35$ keV and the calculated peak value $\sigma(E1) = 152$ μb may be used to determine $\Gamma_\gamma = 0.80$ eV. Our calculation yields $B(E1, {}^{13}\text{C}) = B(E1, {}^{13}\text{N}) = 0.16$ W.u. for the $\frac{1}{2}^+ \to \frac{1}{2}^-$ transition. Thus the change in the $2s_{1/2}$ radial wave functions does not change the strength of this mirror transition. This occurs because the change in normalization of the wave function compensates the change in the tail region.

The binding-energy effect on the $(\frac{3}{2}^-, T = \frac{3}{2}) \to (\frac{1}{2}^+, T = \frac{1}{2})$ decays is not so simple to calculate. The dominant p-shell configuration of the $T = \frac{3}{2}$ level cannot contribute to this decay. Several possible sd-shell admixtures in the $T = \frac{3}{2}$ level may contribute to this decay. All such configurations are bound in the $T = \frac{3}{2}$ level and hence should have similar radial wave functions in ^{13}C and ^{13}N. We have estimated the effect due to only one such configuration, namely ^{12}C(2^-, $T = 1$, 1658 MeV) $\otimes 2s_{1/2}$. The transition then has the form $[1p_{3/2}^{-1}(2s_{1/2}1d)^2]_{T=3/2} \xrightarrow{E1} [2s_{1/2}]$. The $E1$ operator connects one of the $2s1d$-shell nucleons in the $T = \frac{3}{2}$ level with the $1p_{3/2}$ hole. This part of the matrix element should have nearly the same value in ^{13}C and in ^{13}N since only bound wave functions are involved. A binding effect arises from the overlap of the $2s_{1/2}$ nucleons in the initial and final states. The overlap integrals were calculated from the expression

$$I = \left| \int_{r=0}^{30\text{ fm}} u_f^* u_i \, dr \right|^2 .$$

We find $I(^{13}\text{C})/I(^{13}\text{N}) = 1.35$. This leads to an expected asymmetry of $\delta = 0.35$ for the $(\frac{3}{2}^-, T=\frac{3}{2}) \xrightarrow{E1} (\frac{1}{2}^+, T=\frac{1}{2})$ transition, compared to the observed asymmetry of $\delta \geq 0.83 \pm 0.29$. Thus a substantial part of this asymmetry may be due to binding-energy effects and/or isospin mixing in the $T=\frac{3}{2}$ levels.

The discrepancy between the experimental and calculated asymmetries in the $(\frac{1}{2}^+, T=\frac{1}{2}) \rightarrow (\frac{1}{2}^-, T=\frac{1}{2})$ transitions clearly indicates that charge-dependent parentage differences must be present. These differences are not due to isospin mixing (as argued above), but are instead charge-dependent differences in the T-allowed components of the nuclear wave functions. This "dynamic distortion"[39] means that the wave functions of the mirror states are no longer related by the isospin raising or lowering operator. Kurath[40] has recently demonstrated the sensitivity of the $(\frac{1}{2}^+, T=\frac{1}{2}) \rightarrow (\frac{1}{2}^-, T=\frac{1}{2})$ transition to the amount of ^{12}C $(2^+, 4.43) \otimes 1d_{5/2}$ configuration in the $\frac{1}{2}^+$ state (which contributes to the $E1$ decay through the ^{12}C $(2^+, 4.43) \otimes 1p_{3/2}$ component in the ground state). It is clear that the binding-energy difference will make this contribution less important in ^{13}N than in ^{13}C. The amplitude of the (unbound) $2s_{1/2}$ wave function near the nuclear surface is smaller in ^{13}N than ^{13}C, and the coupling potential to the ^{12}C(4.4) $\otimes 1d_{5/2}$ configuration peaks in the surface region. Since the ^{12}C$(4.4) \otimes 1d_{5/2}$ contribution will interfere destructively in the $E1$ matrix element with the contribution from ^{12}C$(0.0) \otimes 2s_{1/2}$, the ^{13}N decay will be retarded less than the ^{13}C decay, as observed experimentally. Recently Fox *et al.*[35] have reproduced the experimental strengths in a coupled-channels calculation which includes the effects discussed above.

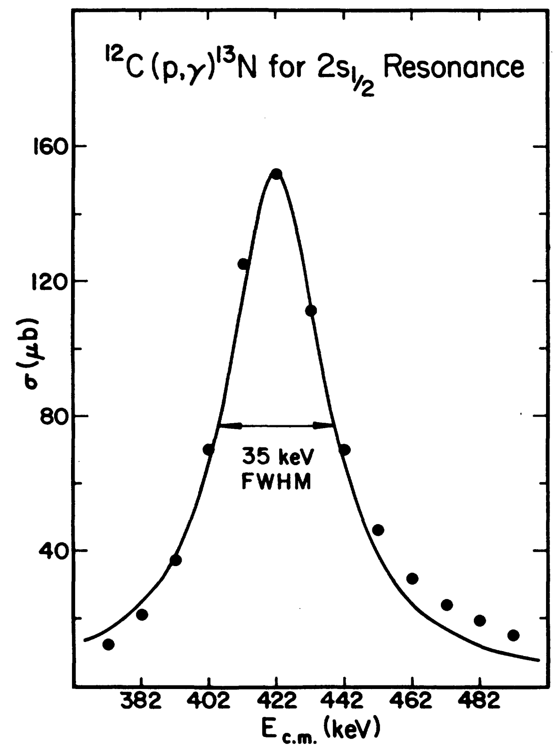

FIG. 14. Resonant ^{12}C$(p,\gamma)^{13}$N cross section for the unbound first excited state in ^{13}N. The points were calculated from scattering wave functions as described in the text. The solid curve is a Breit-Wigner with a width of $\Gamma = 35$ keV, normalized to the calculated point on the peak of the resonance.

V. SUMMARY

The results presented here constitute the most precise available comparison of isovector transitions in mirror nuclei. The mirror $M1$ transitions in mass 13 have the same strength within experimental uncertainties. Thus there is no evidence for either an isotensor component in the electromagnetic interaction or unexpected asymmetries in the nuclear structure of ^{13}C and ^{13}N. The mirror $E1$ transitions in mass 13, on the other hand, show large asymmetries in their strength. The asymmetry in the strongest of the $T=\frac{1}{2} \rightarrow T=\frac{1}{2}$ $E1$ transitions must be due to charge-dependent configuration differences, presumably "dynamic distortions" induced by binding-energy differences. Asymmetries in the other $E1$ transitions are probably due to similar subtle differences in the nuclear structure. The $E1$ decays from the $T=\frac{3}{2}$ levels may have contributions from isospin mixing as well.

ACKNOWLEDGMENTS

We would like to thank J. E. Bussoletti for help in writing the event-mode data handling programs, and M. D. Cooper for participation in early stages of the experiment. We are grateful to D. Kurath and D. Gloeckner for computing shell-model matrix elements for us.

†Work supported in part by U. S. Energy and Research Development Administration.

*Present address: Physics Department, Indiana University, Bloomington, Indiana 47401.

[1]R. E. McDonald, J. A. Becker, R. A. Chalmers, and D. H. Wilkinson, Phys. Rev. C 10, 333 (1974); J. Eichler, T. A. Tombrello, and J. N. Bahcall, Phys. Lett. 13, 146 (1964).

[2]R. J. Blin-Stoyle, Phys. Rev. Lett. 23, 535 (1969).
[3]H. Sato and S. Yoshida, Nucl. Phys. A211, 509 (1973).
[4]M. Chemtob and S. Furui, Nucl. Phys. A233, 435 (1974).
[5]S. Cohen and D. Kurath, Nucl. Phys. 73, 1 (1965).
[6]R. E. Marrs, E. G. Adelberger, K. A. Snover, and M. D. Cooper, Phys. Rev. Lett. 35, 202 (1975).
[7]F. S. Dietrich, M. Suffert, A. V. Nero, and S. S. Hanna, Phys. Rev. 168, 1169 (1968).
[8]M. D. Hasinoff, S. T. Lim, D. F. Measday, and T. J. Mulligan, Nucl. Instrum. Methods 117, 375 (1974).
[9]M. J. Levine and P. D. Parker, Phys. Rev. 186, 1021 (1969).
[10]B. M. Skwiersky, C. M. Baglin, and P. D. Parker, Phys. Rev. C 9, 910 (1974).
[11]M. A. Preston, *Physics of the Nucleus* (Addison-Wesley, Palo Alto, 1962).
[12]H. W. Lewis, Phys. Rev. 125, 937 (1962).
[13]D. G. Costello, J. G. Skofronick, A. L. Morsell, D. W. Palmer, and R. G. Herb, Nucl. Phys. 51, 113 (1964), and references therein.
[14]H. Bichsel, *American Institute of Physics Handbook* (McGraw-Hill, 1972), 3rd. ed., p. 8142; and private communication.
[15]K. A. Snover, Ph.D. thesis, Stanford University, 1969 (unpublished).
[16]E. G. Adelberger, R. E. Marrs, K. A. Snover, and J. E. Bussoletti, Phys. Rev. C 15, 484 (1977).
[17]C. L. Cocke, J. C. Adloff, and P. Chevallier, Phys. Rev. 176, 1120 (1968).
[18]G. Wittwer, H. G. Clerc, and G. A. Beer, Phys. Lett. 30B, 634 (1969).
[19]K. A. Snover, E. G. Adelberger, and F. Riess, Bull. Am. Phys. Soc. 13, 1662 (1968), and (unpublished).
[20]D. P. Balamuth, R. W. Zurmühle, and S. L. Tabor, Phys. Rev. C 10, 975 (1974).
[21]D. E. Alburger and D. H. Wilkinson, Phys. Rev. C 5, 384 (1972).
[22]E. G. Adelberger, A. B. McDonald, C. L. Cocke, C. N. Davids, A. P. Shukla, H. B. Mak, and D. Asbery, Phys. Rev. C 7, 889 (1973).
[23]C. Rolfs and R. E. Azuma, Nucl. Phys. A227, 291 (1974).
[24]D. Gloeckner (private communication).
[25]F. Hinterberger, P. V. Rossen, H. G. Ehrlich, B. Schuller, R. Jahn, J. Bisping, and G. Welp, Nucl. Phys. A253, 125 (1975).
[26]R. E. Marrs, E. G. Adelberger, K. A. Snover, and M. D. Cooper, Nucl. Phys. A256, 1 (1976), and references therein.
[27]See, for example, R. W. Clifft, E. Gabathuler, L. S. Littenberg, R. Marshall, S. E. Rock, J. C. Thompson, and D. L. Ward, Phys. Rev. Lett. 33, 1500 (1974).
[28]D. H. Wilkinson, D. E. Alburger, D. R. Goosman, K. W. Jones, E. K. Warburton, G. T. Garvey, and R. L. Williams, Nucl. Phys. A166, 661 (1971).
[29]K. W. Jones, W. R. Harris, M. T. McEllistrem, and D. E. Alburger, Phys. Rev. 186, 978 (1969).
[30]J. E. Esterl, J. C. Hardy, R. G. Sextro, and J. Cerny, Phys. Lett. 33B, 287 (1970).
[31]S. S. Hanna, in *Isospin in Nuclear Physics*, edited by D. H. Wilkinson (North-Holland, Amsterdam, 1969).
[32]D. Kurath (private communication).
[33]F. J. Ajzenberg-Selove, Nucl. Phys. A152, 1 (1970).
[34]S. W. Robinson, C. P. Swann, and V. K. Rasmussen, Phys. Lett. 26B, 298 (1968); F. Metzger (private communication).
[35]G. Fox, J. G. Polchinski, C. Rolfs, and T. A. Tombrello (unpublished).
[36]E. H. Auerbach, Brookhaven National Laboratory (unpublished).
[37]Amos de-Shalit and Igal Talmi, *Nuclear Shell Theory* (Academic, New York, 1963).
[38]R. F. Christy and I. Duck, Nucl. Phys. 24, 89 (1961).
[39]W. M. McDonald, in *Nuclear Spectroscopy* B, edited by F. Ajzenberg-Selove (Academic, New York, 1960), p. 932.
[40]D. Kurath, Phys. Rev. Lett. 35, 1546 (1975).